Vesicle Trafficking and Cell Surface Membrane Patchiness

Qing Tang and Michael Edidin
Department of Biology, The Johns Hopkins University, Baltimore, Maryland 21218 USA

ABSTRACT Membrane proteins and lipids often appear to be distributed in patches on the cell surface. These patches are often assumed to be membrane domains, arising from specific molecular associations. However, a computer simulation (Gheber and Edidin, 1999) shows that membrane patchiness may result from a combination of vesicle trafficking and dynamic barriers to lateral mobility. The simulation predicts that the steady-state patches of proteins and lipids seen on the cell surface will decay if vesicle trafficking is inhibited. To test this prediction, we compared the apparent sizes and intensities of patches of class I HLA molecules, integral membrane proteins, before and after inhibiting endocytic vesicle traffic from the cell surface, either by incubation in hypertonic medium or by expression of a dominant-negative mutant dynamin. As predicted by the simulation, the apparent sizes of HLA patches increased, whereas their intensities decreased after endocytosis and vesicle trafficking were inhibited.

INTRODUCTION

The current minimal model of cell membranes, the fluid mosaic model, emphasizes the mobility and autonomy of membrane proteins and lipids (Singer and Nicolson, 1972). In this model there is no lateral organization (Sadava, 1992), though diffusing molecules may collide and interact in the plane of the membrane. The model is based upon studies of the composition of membrane proteins and on early, qualitative, demonstrations that membrane proteins diffuse in the plane of the membrane.

A second model of membrane organization has developed in the past two decades. The model emphasizes the lateral organization of membranes into domains with long-range order, over hundreds of nanometers, in the lipid bilayer. The model is based upon studies of synthetic lipid bilayers (Jain and White, 1977), but it is also consistent with the quantitative details of lateral mobility of proteins in membranes. Though there is no single summary of the model, recent reviews of membrane lipid domains (Brown and London, 2000; Edidin, 1997; Moffett et al., 2000) and of protein diffusion (Saxton and Jacobson, 1997) imply that cell surface membranes are rich in patches of lipids and proteins on many size (and time) scales. Such patches are often seen after labeling surfaces with fluorescent tags for either proteins or lipids. High-resolution near-field scanning optical microscopy (NSOM) images of labeled cell surfaces also show patches of lipids and proteins on many scales (Hwang et al., 1998).

Lipid domains may form due to specific associations among their components (the best example of this being so-called lipid rafts) (Brown and London, 1998; Simons and Ikonen, 2000), whereas the patches of protein, for example those observed by NSOM, are of a size, ~300 nm, typical of membrane corrals confining and limiting lateral diffusion of membrane proteins (Sheetz, 1983; Sheetz et al., 1980). We might expect lipid domains to be small and transient (Edidin, 1997), particularly since the energies of interaction between phospholipids are small compared with the energies involved in trafficking molecules to and from the cell surface. We also might expect patches of proteins to be short lived, because the barriers to their diffusion open transiently on a time scale of seconds (Saxton and Jacobson, 1997).

To understand the connection between the frequency of crossing barriers to lateral mobility and the appearance of patches of membrane proteins, we have simulated a cell surface membrane using literature data on lateral diffusion, frequency, and stability of barriers to lateral mobility, and vesicle traffic between cell surface membrane and cell interior (Gheber and Edidin, 1999). In the model, we found that vesicle traffic to and from the cell surface and dynamic barriers to the lateral diffusion resulted in a membrane rich in patches at steady state. If barriers were removed, patches decayed by diffusion of their components. The patches also decayed if vesicle traffic was blocked, because barriers to lateral diffusion were not stable for more than tens of seconds.

The model predicts that patches of protein imaged in labeled cell surfaces will decay, increasing in patch size and decreasing in intensity per unit area, if vesicle trafficking is inhibited. Here we show that this is indeed the case. We first characterize the apparent size and fluorescent intensity (corresponding to number of molecules) of patches of class I HLA molecules, integral membrane proteins, labeled with fluorescent monovalent label (Fab). We then show that if endocytosis is inhibited, the intensity of the patches falls while the apparent patch size increases.

MATERIALS AND METHODS

Materials

Unlabeled Polybead carboxylate microspheres (Polysciences, Warrington, PA), 50 or 100 nm in diameter, are monodispersed polystyrene latex

Received for publication 26 September 2000 and in final form 31 March 2001.

Address reprint requests to Dr. Michael Edidin, Department of Biology, The Johns Hopkins University, 3400 North Charles Street, Baltimore, MD 21218-2685. Tel.: 410-516-7294; Fax: 410-516-5213; E-mail: edidin@jhu.edu.

0006-3495/01/07/196/08 $2.00

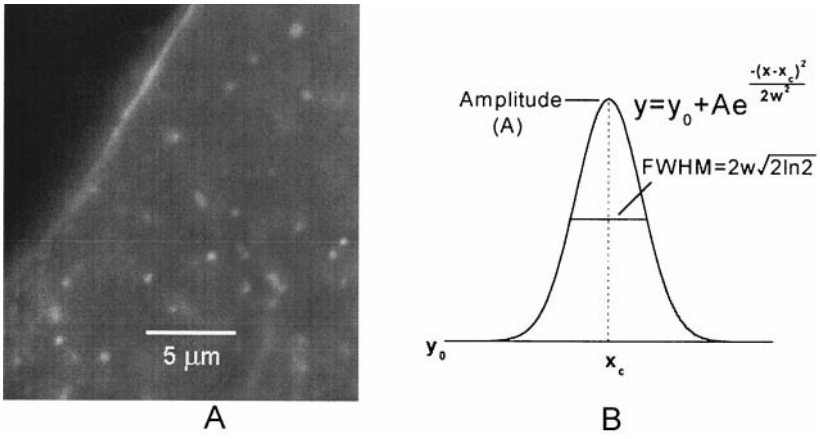

FIGURE 1 Sample conventional fluorescence microscopy CCD image and Gaussian function fit. (*A*) A sample image of class I HLA patches on the surface of fibroblasts; (*B*) A typical Gaussian function fit of the profile of a fluorescent spot in the images. The apparent size of a patch is taken from full width at half-maximum amplitude (FWHM), and the intensity from integrated fluorescence volume under the Gaussian function fit.

particles that contain surface carboxyl groups. Fluoresbrite yellow green (YG) carboxylate microspheres (458-nm excitation, 540-nm emission, Polysciences), 50 nm in diameter, are fluorescent monodispersed polystyrene microspheres. KE2 is an IgG monoclonal antibody of HLA molecules (Schreiber et al., 1984). KE2 Fab was prepared as described elsewhere (Edidin and Wei, 1982) and conjugated with Cy3 (552-nm excitation, 565-nm emission, Amersham Pharmacia Biotech, Piscataway, NJ) following the manufacturer's directions. The dye:protein ratio of the Cy3-KE2 conjugate was 1:1 (from here on KE2 refers to KE2 Fab, unless otherwise indicated). The fluorescence of solutions of diluted conjugate increased linearly over the range 1–20 nM.

Cy3-KE2 was bound to Polybeads and KE2 Fab was bound to Fluoresbrite beads according to the manufacturer's directions (Polysciences, Technical Data Sheet 238), except that free protein was separated from beads by passing the mixture through Sephadex G-200 (Pharmacia Fine Chemicals, Piscataway, NJ).

Normal human skin fibroblasts, 5659C (National Institute of General Medical Sciences Cell Repository, Coriell Institute, Camden, NJ), were cultured at 37°C in Eagle's minimal essential medium (MEM; Molecular Research Laboratories, Herndon, VA) with 20% fetal bovine serum (FBS; Life Technologies Inc, Grand Island, NY), 1% non-essential amino acids (Life Technologies) and 1% vitamins (Life Technologies). HeLa cells expressing either wild-type dynamin (dyn^{wt}) or temperature-sensitive mutant dynamin (dyn^{ts}) (Damke et al., 1995) were kindly provided by Dr. Sandra L. Schmid (The Scripps Research Institute, La Jolla, CA). HeLa cells were cultured at 37°C in Dulbecco's modified MEM (DMEM; Life Technologies) with 10% FBS, 100 U/ml antibiotic/antimycotic (Life Technologies), 400 μg/ml G418 (Geneticin; Sigma, St. Louis, MO), 2 μg/ml tetracycline (Sigma), and 200 ng/ml puromycin (Sigma).

Hypertonic treatment and cell labeling

Fibroblasts were incubated in hypertonic medium (MEM, 0.45 M sucrose) for 15 min or 1 h. Control cells were incubated in MEM. After incubation, cells were labeled with excess Cy3-KE2 on ice for 1 h, fixed in freshly prepared 4% paraformaldehyde (Electron Microscopy Sciences, Fort Washington, PA), and imaged.

Temperature shift

Dyn^{wt} and dyn^{ts} HeLa cells were induced for dynamin expression by growth in DMEM without tetracycline for 72 h at 30°C and then shifted from 30°C to 38°C for 15 min or 1 h. Control cells were incubated at 30°C. After incubation, cells were labeled with excess Cy3-KE2, fixed, and imaged.

Intensity calibration

Different amounts of bead suspension (0.0625, 0.125, 0.25, 0.5, and 1 μl) were incubated with 10 μl of Cy3-KE2 for 1 h at room temperature. They were then centrifuged at 80,000 $\times$ *g* for 30 min. The supernatant was diluted to yield a solution with the concentration between 1 and 20 nM in Cy3-KE2, a range where there was a linear relationship between Cy3-KE2 concentration and fluorescence. The amount of Cy3-KE2 bound by the beads was determined in terms of the difference between the fluorescence of the Cy3-KE2 solution before incubation with beads and the fluorescence of supernatant after incubation. The amount of Cy3-KE2 bound on beads increased linearly with the amount of beads added. From these data, and knowing the concentration of the beads themselves, we calculated that each 50-nm bead bound ~40 Cy3-KE2 molecules. This compares well with the number of IgG molecules, ~25–30, reported to be bound to one 40-nm colloidal gold particle (de Brabander et al., 1991) and the number of IgG molecules, ~40, bound to one 50-nm plastic bead (Edidin et al., 1994).

Cy3-KE2 (5 μM) or Cy3-KE2/KE2 mix (1:1, 2.5 μM each) was incubated with 50-or 100-nm plain beads. The 50-nm or 100-nm beads with two different amounts of Cy3-KE2 bound on the bead surface were then imaged separately. All the beads were imaged on coverslips. Cells labeled with Cy3-KE2 were imaged under same conditions (exposure time and gain) to determine the number of HLA molecules per labeled HLA cluster.

Measurement of fluid-phase endocytosis

Fibroblasts were treated in hypertonic medium for various times (5, 10, 25, and 55 min). Cells were then washed twice in PBS and incubated with 4 mg/ml horseradish peroxidase (HRP; Sigma) in MEM, 0.45 M sucrose, 20 mM Hepes, 0.2% bovine serum albumin (BSA), pH 7.4, for another 5 min (Damke et al., 1995). To terminate the uptake, cells were washed six times with PBS, 1 mM $MgCl_2$, 1 mM $CaCl_2$, 0.2% BSA, pH 7.4, for 5 min at 4°C. After two additional washes with PBS, cells were typsinized and centrifuged in PBS with 0.5 M sucrose for 5 min at 1000 $\times$ *g* at 4°C. The cells were then solubilized in PBS, 0.5% Triton X-100. O-phenylene diamine (OPD; 0.4 mg/ml, Sigma) was used as substrate to measure HRP activity in an aliquot of the cells. Another aliquot of the cells was used to measure total protein by BCA assay (Pierce, Rockford, IL) (Damke et al., 1995). The ratio of HRP activity to total protein gave the HRP uptake by cells. Uptake of HRP by cells incubated in normal medium was taken as the 100% control.

Dyn^{wt} and Dyn^{ts} HeLa cells were shifted from permissive temperature to nonpermissive temperature for various times (5, 10, 25, and 55 min). Cells were then washed twice in PBS and incubated with 4 mg/ml HRP in

DMEM, 20 mM Hepes, 0.2% BSA, pH 7.4, for another 5 min. HRP uptake was then measured as described above.

Image acquisition and analysis

For most experiments, fluorescence images were taken on a Zeiss Axiovert 135 TV conventional inverted microscope (Carl Zeiss, Thornwood, NY) equipped with a cooled slow-scan CCD camera (Series 300, Photometrics, Tucson, AZ), a 100×1.4 NA oil DIC objective (Plan-Apochromat, Zeiss) and a 75-W xenon arc lamp epi-illumination. The CCD image is 1317 × 1035 pixels corresponding to 68 nm/pixel with 100× objective. After calibration with fluorescent beads, as described in Results, constant camera exposure time and gain were used for all CCD images. Cells and beads were also imaged on a Leica TCS-NT laser confocal microscope (Leica Microsystems, Exton, PA).

An interactive program was written in IDL software (Research Systems, Boulder, CO) to evaluate fluorescent patches in the images (Fig. 1 *A*). Patches around the limit of microscope resolution in apparent size were fit by a Gaussian function. The apparent size was taken from the full width at half-maximum amplitude (FWHM) of the Gaussian fit (Fig. 1 *B*). The intensity was the integrated fluorescence volume under the Gaussian fit. The data were compiled from many samples (beads and cells) and statistically analyzed by Origin software (OriginLab Co., Northampton, MA).

RESULTS

Number of HLA molecules in a patch

We first imaged 50-nm plain beads coated with Cy3-KE2 in a conventional fluorescence microscope equipped with a cooled CCD camera. The beads, whose size is well below the spatial resolution of the microscope, appeared as spots with an apparent size of some hundreds of nanometers. Each fluorescent spot was fit by a Gaussian function, and the apparent size was taken from the FWHM of each Gaussian fit. The apparent size distribution of the population of beads is shown in Fig. 2 *A*. The mean apparent size (±SD) of beads was 318.6 nm (±20.4 nm). The intensity of each spot was the integrated fluorescence volume under the Gaussian fit. The intensity distribution is shown in Fig. 2 *B*. The beads were monodispersed microspheres, and we believe that the highest peak at ~450 arbitrary fluorescence units (afu) in the distribution arose from single beads. That is to say, ~450 afu is the intensity of one single bead that binds ~40 Cy3-KE2 on the bead surface.

Next we imaged HLA molecules on the surface membranes of HeLa cells labeled with excess Cy3-KE2. The apparent size distribution (Fig. 2 *C*) of HLA patches was somewhat broader than that of beads. The mean apparent size (±SD) was 321.7 nm (±36.7 nm), not significantly different from the mean apparent size of beads. The intensity distribution of HLA clusters (Fig. 2 *D*) ranged from 250 to 2750 afu. Using the fact that ~40 molecules of Cy3-KE2 yield ~450 afu, we estimate that an HLA cluster contains ~20–240 molecules (assuming no steric hindrance to binding of our Fab), which is consistent with our earlier measurements. (Chakrabarti et al., 1992; Hwang et al., 1998).

We also imaged 50-nm plain beads on a coverslip and HLA clusters on normal fibroblasts labeled with Cy3-KE2 by scanning laser confocal microscopy (SLCM). The mean apparent size of beads was ~280 nm, smaller than the mean apparent size in the conventional microscopy CCD images. The calibrated intensity for one bead was ~900 afu under optimal imaging parameters. The intensity distribution of

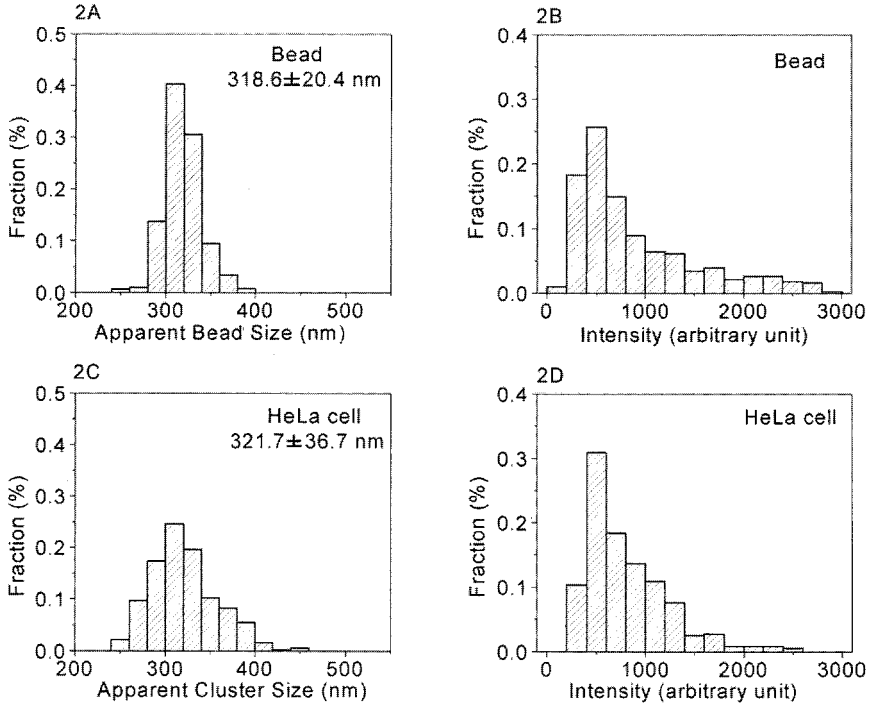

FIGURE 2 Apparent size and intensity distributions of 50-nm beads and class I HLA patches on dyn^{wt} HeLa cells. (*A*) Apparent size distribution of beads; (*B*) Intensity distribution of beads; (*C*) Apparent size distribution of HLA patches on dyn^{wt} HeLa cells; (*D*) Intensity distribution of HLA patches on HeLa cells.

HLA clusters on fibroblast cells ranged from 300 to 4500 afu, leading to an estimate of ~15–200 molecules per HLA cluster, within the range estimated above by conventional microscopy.

The spatial resolution of SLCM is better than that of our CCD microscope. However, in later experiments, we chose to use the CCD microscope, because it had better signal/noise ratio and caused less sample photobleaching than the SLCM.

Intensities and apparent sizes of different bead/Cy3-KE2 combinations

Cy3-KE2 or Cy3-KE2/KE2 mix (1:1) was incubated with 50- or 100-nm plain beads. This Cy3-KE2/KE2 mix was expected to give half the fluorescence per bead (50 or 100 nm) as undiluted Cy3-KE2.

The mean apparent sizes and intensities for four bead/Cy3-KE2 combinations are shown in Table 1. Neither 50- nor 100-nm beads appeared to change apparent size as different amounts of Cy3-KE2 bound on the bead surfaces. Also, the apparent size of 50-nm beads appeared no different from that of 100-nm beads. Fluorescence intensity per bead increased with increasing ratio of Cy3-KE2 in the incubation mixture. The apparent size of the 50-nm beads was the same as that of 100-nm beads (318.6 ± 20.4 nm vs. 324.2 ± 18.1 nm), and these sizes did not change as intensity increased.

Because the surface area of one 100-nm bead is four times larger than that of one 50-nm bead, one would expect that the intensities of 100-nm beads is four times higher than that of 50-nm beads. However, the intensity peak of 100-nm beads with Cy3-KE2 (or Cy3-KE2/KE2 mix) is only about two times higher than that of 50-nm beads. This is probably because Cy3-KE2 did not saturate the surface of 100-nm beads. Nevertheless, for either 50-or 100-nm beads, the more Cy3-KE2 bound on the surface, the higher was the fluorescence intensity per bead.

Inhibition of clathrin-dependent endocytosis by hypertonic treatment

A 15-min hypertonic treatment had the greatest effect on endocytosis measured in terms of uptake of HRP. With longer incubation times, 30 min or 1 h, endocytosis gradually recovered. This is likely due to a compensatory increase in endocytosis by clathrin-independent pathways (Heuser and Anderson, 1989). In the experiments that follow, cells were treated in hypertonic medium for either 15 min or 1 h.

Fig. 3 shows the apparent size and intensity distributions of HLA clusters after cells were treated for 15 min and 1 h in hypertonic medium (and labeled with Cy3-KE2). It can be seen that the distribution of apparent sizes of HLA patches broadened and shifted to larger sizes after a 15-min treatment of cells with hypertonic medium. Statistical comparison of the results shows that the mean intensity of the patches decreased after a 15-min incubation of cells in hypertonic medium (Table 2). Thus, when traffic of clathrin-coated vesicles was inhibited for 15 min, HLA patches were on the average larger and dimmer than those on control cells. After 1 h, when endocytosis had returned to the level seen in controls, the distributions of apparent sizes and intensities of HLA patches were similar to that of control cells.

Inhibition of clathrin-dependent endocytosis by expression of mutant dynamin

Dynamin is a key component of clathrin-mediated endocytosis (Sever et al., 2000). Phenotypic characterization of the cells transformed with mutant dynamin established that dynamin function is required for pinching off of coated pits at the plasma membrane (Damke et al., 1994; Sever et al., 2000). Damke and co-workers (1995) also showed that when a stable HeLa cell line expressing temperature-sensitive dynamin mutant was shifted from permissive temperature to nonpermissive temperature, clathrin-dependent endocytosis was inhibited.

For dyn^{ts} HeLa cells, our measurement of HRP uptake showed that, as has been reported (Damke et al., 1995), a 15-min incubation at nonpermissive temperature had the greatest effect on fluid-phase endocytosis (data not shown). After 30 min or 1 h of incubation at nonpermissive temperature, fluid-phase endocytosis recovered to the level of control cells. The temperature shift had no effect on HRP uptake by dyn^{wt} HeLa cells.

Fig. 4 shows the distributions of apparent sizes and intensities of HLA patches on dyn^{ts} HeLa cells at both permissive and nonpermissive temperatures. It shows that the distribution of patch sizes is broadened and shifted to larger

TABLE 1 Student's *t*-tests of apparent size and intensity of different bead/Cy3-KE2 combinations

Bead/Cy3-KE2 combination (nm/μM)	Apparent size ± SD (nm)	Apparent size *t*-test*	Ln (intensity) ± SD (arbitrary unit)	Intensity *t*-test*	*N*
50/5	319.5 ± 21.7		6.28 ± 0.25		225
50/2.5	318.0 ± 26.1	0.60	5.74 ± 0.37	16.65	145
100/5	324.2 ± 18.1		6.78 ± 0.30		608
100/2.5	326.5 ± 26.3	1.36	6.25 ± 0.61	18.67	466

*Versus control.

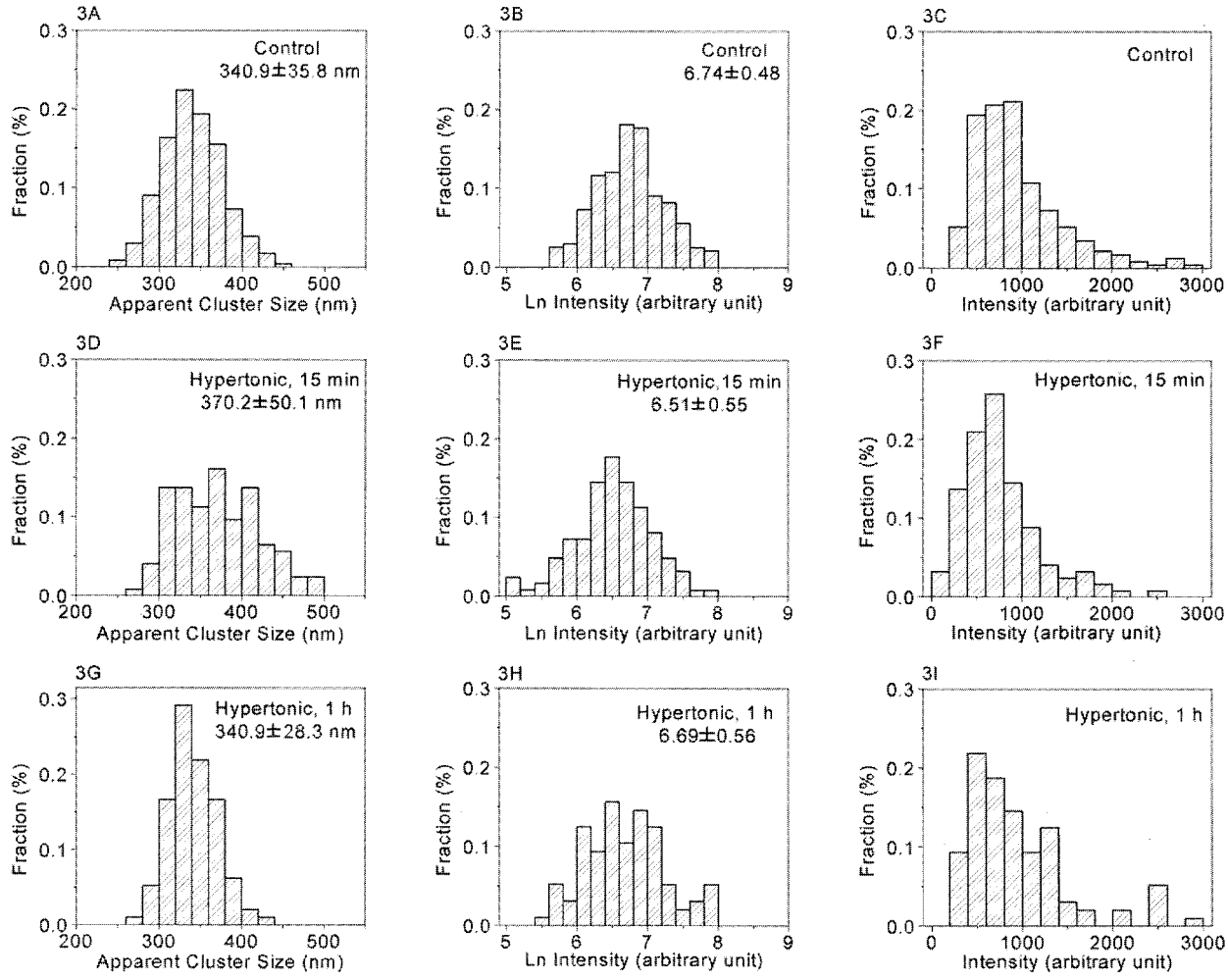

FIGURE 3 Apparent size and intensity distributions of HLA clusters after fibroblasts were treated for 15 min or 1 h in hypertonic medium. (*A–C*) Cells were incubated with normal medium; (*D–F*) Cells were incubated in hypertonic medium for 15 min; (*G–I*) Cells were incubated in hypertonic medium for 1 h. In the first column are apparent size distributions; in the second column, intensity distributions were plotted in logarithm *x* axis; in the third column, intensity distributions were plotted in linear *x* axis.

sizes after 15 min at 38°C and returns to that of controls after 1 h at 38°C. There is also a large shift to lower intensities after 15 min. The statistical comparisons of the means for the distributions are given in Table 3.

Shifting dyn^{wt} HeLa cells from 30°C to 38°C had no effect on HLA patch apparent size or intensity (Table 3).

Apparent size simulation

In both treatments used above, we saw changes in apparent sizes of HLA patches. However, the apparent size should remain the same if the true patch size remains below the resolution limit of the microscope. To clarify this, we did a

TABLE 2 Student's *t*-tests of apparent size and intensity of HLA clusters after cells were treated in hypertonic medium for 15 min or 1 h

Label	Hypertonic treatment (min)	Apparent size ± SD (nm)	Apparent size *t*-test*	Ln (intensity) ± SD (arbitrary unit)	Intensity *t*-test*	*N*
Cy3-KE2	0 (control)	340.9 ± 35.8		6.74 ± 0.48		232
	15	370.2 ± 50.1	6.37	6.51 ± 0.56	4.22	124
	60	340.9 ± 28.3	0.01	6.69 ± 0.56	0.85	96
KE2 Fab-coated fluorescent bead	0 (control)	309.4 ± 29.2		6.70 ± 0.42		246
	15	305.5 ± 32.0	1.50	6.66 ± 0.44	1.14	322

*Versus control.

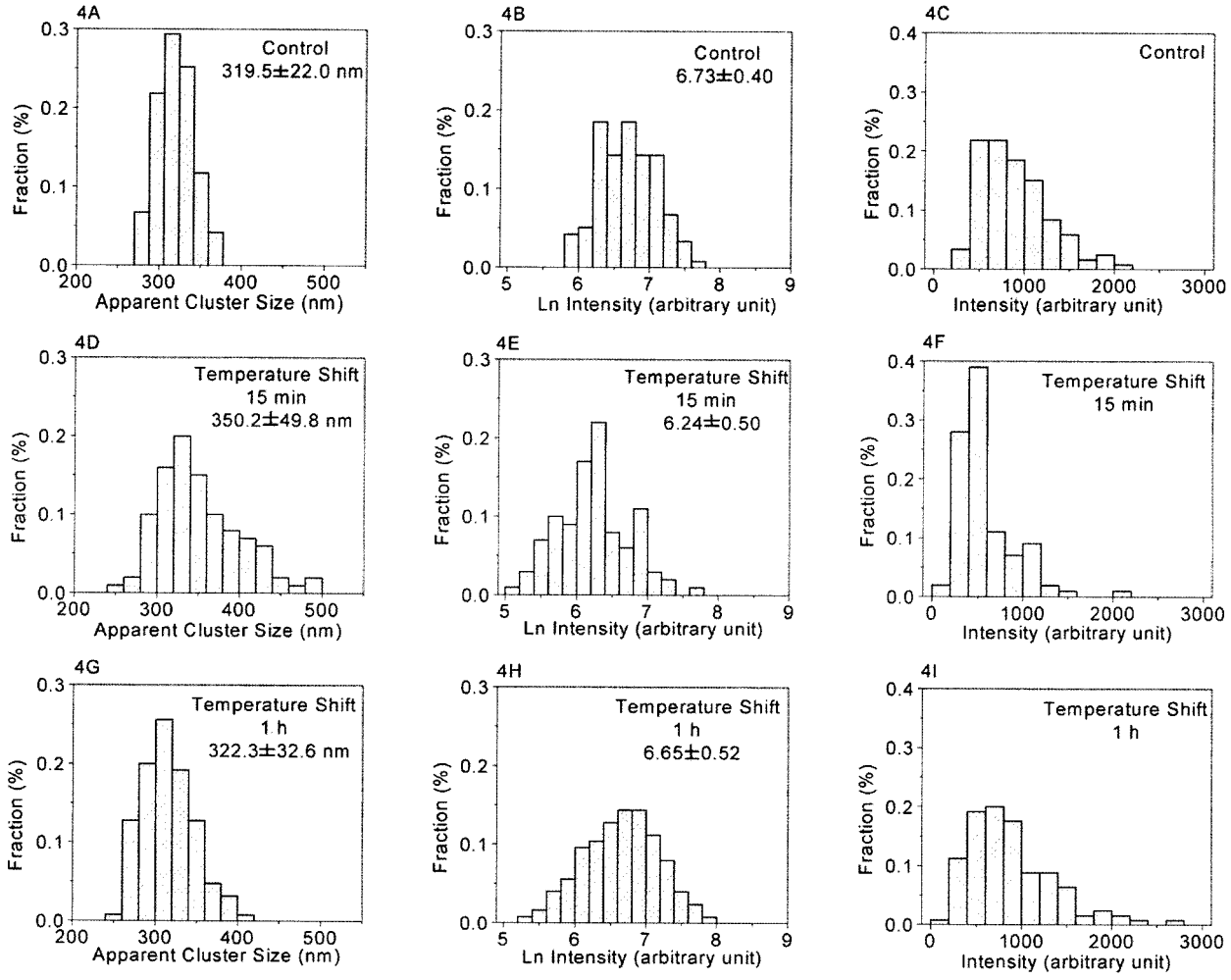

FIGURE 4 Apparent size and intensity distributions of HLA clusters after dyn^{ts} HeLa cells were shifted from 30°C to 38°C for 15 min or 1 h. (*A–C*) Cells were incubated at 30°C; (*D–F*) Cells were shifted to 38°C for 15 min; (*G–I*) Cells were shifted to 38°C for 1 h. In the first column are apparent size distributions; in the second column, intensity distributions were plotted in logarithm *x* axis; in the third column, intensity distributions were plotted in linear *x* axis.

simulation of apparent size versus real size for patches over the range 25–260 nm (Fig. 5). The apparent sizes were calculated as the convolution of real size and an ideal point-spread function with a 260-nm microscope resolution. From this simulation, one can see that when the real size of a patch is greater than half of the resolution limit (in the simulation, half of 260 nm), it would be possible to detect changes in real size in terms of changes in apparent sizes.

TABLE 3 Student's *t*-tests of apparent size and intensity of HLA clusters after dyn^{ts} and dyn^{wt} HeLa cells were shifted from 30°C to 38°C for 15 min or 1 h

	Label	Temperature shift (min)	Apparent size ± SD (nm)	Apparent size *t*-test*	Ln (intensity) ± SD (arbitrary unit)	Intensity *t*-test*	*N*
Dyn^{ts} HeLa cells	Cy3-KE2	0 (control)	319.5 ± 22.0		6.73 ± 0.40		119
		15	350.2 ± 49.8	6.06	6.24 ± 0.50	8.04	100
		60	322.3 ± 32.6	0.78	6.65 ± 0.52	1.39	125
	KE2 Fab-coated fluorescent Bead	0 (control)	302.8 ± 24.3		6.74 ± 0.48		108
		15	301.4 ± 25.0	0.44	6.76 ± 0.45	0.32	131
Dyn^{wt} HeLa cells	Cy3-KE2	0 (control)	324.7 ± 19.3		6.97 ± 0.28		104
		15	323.2 ± 17.6	0.53	6.95 ± 0.28	0.48	71

*Versus control.

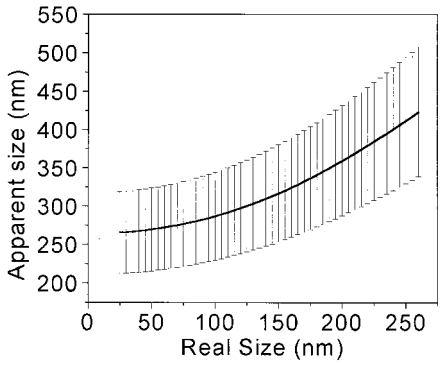

FIGURE 5 Apparent size simulation (with ±20% error). The apparent sizes were calculated as the convolution of real size and an ideal point-spread function with a 260-nm microscope resolution.

This accounts for the increased apparent sizes after treatments in our experiments.

Imaging cells labeled with fluorescent beads

The changes in apparent sizes and intensity that we observed could be caused by some of the patches going out of focus, due to change in cell morphology consequent to treatments inhibiting endocytosis. To see whether this occurred we labeled cells with fluorescent beads coated with KE2 instead of with Cy3-KE2. There was no change in mean apparent size and intensity of fluorescent beads between cells treated with hypertonic medium and control cells (Table 2). There was also no change in the mean apparent size and intensity of fluorescent beads bound to cells after inducing dominant-negative mutant dynamin (Table 3). These two results indicate that changes in cell morphology cannot account for the observed change in apparent size and intensity of HLA patches.

DISCUSSION

The experiments presented here test a model for the creation and maintenance of a membrane with patchy distribution of its components (Gheber and Edidin, 1999). The model simulation predicted that vesicle trafficking and dynamic barriers to lateral mobility are required and sufficient to create and maintain membrane patchiness. It was not necessary to assume specific molecular associations or, indeed, even to assume that vesicles delivering cargo to the surface concentrate this cargo above its average concentration in the membrane. The only assumption made was that membrane area remained constant, so that equal areas of membrane were delivered and removed per unit time.

Our model predicted that if vesicle trafficking to and from the cell surface was blocked, patches of membrane proteins would decay, increasing in size and decreasing in intensity. In the present paper we have tested this prediction using two different methods to inhibit clathrin-dependent endocytosis and, by implication, vesicle delivery. The first method used was hypertonic treatment. Incubation in hypertonic medium inhibited clathrin-dependent endocytosis by blocking formation of clathrin-coated pits and vesicles (Heuser and Anderson, 1989). The second method also inhibited traffic mediated by clathrin-coated pits and vesicles, through expression of a mutant dynamin. Dynamin is required for pinching off of clathrin-coated vesicles. Shifting dyn^{ts} HeLa cell from permissive temperature to nonpermissive temperature makes dynamin not functional, thus preventing clathrin-coated vesicles from budding. This blocks traffic at a slightly later stage than hypertonic medium (Damke et al., 1994; McNiven, 1998; Sever et al., 2000).

Both treatments measurably reduced fluid-phase uptake by cells, an indication that some endocytic vesicle traffic was inhibited (Heuser and Anderson, 1989). However, neither treatment absolutely blocked endocytosis. Furthermore, as has been reported earlier (Damke et al., 1995; Heuser and Anderson, 1989), after 1 h of treatment, the cells' endocytic activity recovered to control levels. This reflects a compensatory increase in traffic of vesicles that are not clathrin dependent (Damke et al., 1995).

Patches of class I HLA molecules were imaged by a conventional fluorescence microscope equipped with a cooled CCD camera. Our NSOM images of such patches (Hwang et al., 1998) as well as other work on class I and class II major histocompatibility complex molecules (Cherry et al., 1998) showed that the size of these patches is at or below the limit of resolution of the light microscope. However, one can distinguish fluorescent spots of different intensities and assign them to different numbers of fluorophores (Gross and Webb, 1986). To verify this in our system, we did control experiments with 50-nm and 100-nm plain beads that were coated with two different amounts of Cy3-KE2. The results showed that, for either 50- or 100-nm beads, the intensities became higher, although the apparent sizes remained the same, as beads were coated with increasing amounts of Cy3-KE2. This allowed us to estimate that there are 20–240 HLA molecules in one HLA cluster on the cell surface membrane. This estimate is consistent with our earlier measurement (Chakrabarti et al., 1992; Hwang et al., 1998).

Despite effecting only a partial block of vesicle traffic we found that our treatments produced a change in the apparent size and intensity of patches of class I HLA molecules. When vesicle traffic was inhibited, patches appeared larger and dimmer than patches in control cells or in cells that had recovered from treatment.

For an ideal case, with very high signal-to-noise ratio, an increase in patch size by diffusion should not change the integrated intensity of the patch. However, at lower signal-to-noise ratio, diffusional broadening will result in fluorescence of the low concentration of labeled molecules at the

edge of the patch being lost in the background noise, autofluorescence, fluorescence from molecules diffusing from patches, as well as electronic noise. Hence, the changes in intensity that we observed suggest that we underestimated changes in patch diameter when vesicle traffic is inhibited.

Thus, despite the resolution limit of the microscope, we were still able to observe the changes in apparent size and intensity of HLA patches after inhibiting endocytosis. These changes are consistent with the prediction of our model (Gheber and Edidin, 1999), that nanometer-scale patches of proteins (and lipids) observed at the cell surface are transient and do not necessarily involve specific lateral interactions between their constituents.

We thank Dr. Sandra L. Schmid for dyn^{ts} and dyn^{wt} HeLa cells. We also thank Taiyin Wei and Andrew Nechkin for technical assistance.

This work was supported by National Institutes of Health grant GM58554 to M.E.

REFERENCES

Brown, D. A., and E. London. 1998. Functions of lipid rafts in biological membranes. *Annu. Rev. Cell. Dev. Biol.* 14:111–136.

Brown, D. A., and E. London. 2000. Structure and function of sphingolipid- and cholesterol-rich membrane rafts. *J. Biol. Chem.* 275: 17221–17224.

Chakrabarti, A., J. Matko, N. A. Rahman, B. G. Barisas, and M. Edidin. 1992. Self-association of class I major histocompatibility complex molecules in liposome and cell surface membranes. *Biochemistry.* 31: 7182–7189.

Cherry, R. J., K. M. Wilson, K. Triantafilou, P. O'Toole, I. E. Morrison, P. R. Smith, and N. Fernandez. 1998. Detection of dimers of dimers of human leukocyte antigen (HLA)-DR on the surface of living cells by single-particle fluorescence imaging. *J. Cell. Biol.* 140:71–79.

Damke, H., T. Baba, A. M. van der Bliek, and S. L. Schmid. 1995. Clathrin-independent pinocytosis is induced in cells overexpressing a temperature-sensitive mutant of dynamin. *J. Cell. Biol.* 131:69–80.

Damke, H., T. Baba, D. E. Warnock, and S. L. Schmid. 1994. Induction of mutant dynamin specifically blocks endocytic coated vesicle formation. *J. Cell. Biol.* 127:915–34.

de Brabander, M., R. Nuydens, A. Ishihara, B. Holifield, K. Jacobson, and H. Geerts. 1991. Lateral diffusion and retrograde movements of individual cell surface components on single motile cells observed with Nanovid microscopy. *J. Cell. Biol.* 112:111–124.

Edidin, M. 1997. Lipid microdomains in cell surface membranes. *Curr. Opin. Struct. Biol* 7:528–532.

Edidin, M., and T. Wei. 1982. Lateral diffusion of H-2 antigens on mouse fibroblasts. *J. Cell. Biol.* 95:458–462.

Edidin, M., M. C. Zuniga, and M. P. Sheetz. 1994. Truncation mutants define and locate cytoplasmic barriers to lateral mobility of membrane glycoproteins. *Proc. Natl. Acad. Sci. U.S.A.* 91:3378–3382.

Gheber, L. A., and M. Edidin. 1999. A model for membrane patchiness: lateral diffusion in the presence of barriers and vesicle traffic. *Biophys. J.* 77:3163–3175.

Gross, D., and W. W. Webb. 1986. Molecular counting of low-density lipoprotein particles as individuals and small clusters on cell surfaces. *Biophys. J.* 49:901–911.

Heuser, J. E., and R. G. Anderson. 1989. Hypertonic media inhibit receptor-mediated endocytosis by blocking clathrin-coated pit formation. *J. Cell. Biol.* 108:389–400.

Hwang, J., L. A. Gheber, L. Margolis, and M. Edidin. 1998. Domains in cell plasma membranes investigated by near-field scanning optical microscopy. *Biophys. J.* 74:2184–2190.

Jain, M. K., and H. B. White. 1977. Long-range order in biomembranes. *Adv. Lipid Res.* 15:1–60.

McNiven, M. A. 1998. Dynamin: a molecular motor with pinchase action. *Cell.* 94:151–154.

Moffett, S., D. A. Brown, and M. E. Linder. 2000. Lipid-dependent targeting of G proteins into rafts. *J. Biol. Chem.* 275:2191–2198.

Sadava, D. E. 1992. Cell Biology: Organelle Structure and Function. Jones and Bartlett, Boston, MA

Saxton, M. J., and K. Jacobson. 1997. Single-particle tracking: applications to membrane dynamics. *Annu. Rev. Biophys. Biomol. Struct.* 26: 373–399.

Schreiber, A. B., J. Schlessinger, and M. Edidin. 1984. Interaction between major histocompatibility complex antigens and epidermal growth factor receptors on human cells. *J. Cell Biol.* 98:725–731.

Sever, S., H. Damke, and S. L. Schmid. 2000. Dynamin:GTP controls the formation of constricted coated pits, the rate limiting step in clathrin-mediated endocytosis. *J. Cell Biol.* 150:1137–1148.

Sheetz, M. P. 1983. Membrane skeletal dynamics: role in modulation of red cell deformability, mobility of transmembrane proteins, and shape. *Semin. Hematol.* 20:175–188.

Sheetz, M. P., M. Schindler, and D. E. Koppel. 1980. Lateral mobility of integral membrane proteins is increased in spherocytic erythrocytes. *Nature.* 285:510–511.

Simons, K., and E. Ikonen. 2000. How cells handle cholesterol. *Science.* 290:1721–1726.

Singer, S. J., and G. L. Nicolson. 1972. The fluid mosaic model of the structure of cell membranes. *Science.* 175:720–731.